Depth sectioning of attenuation

Keith Dillon* and Yeshaiahu Fainman

Department of Electrical and Computer Engineering, University of California–San Diego, 9500 Gilman Drive, La Jolla, California 92093-0407, USA
**Corresponding author: kdillon@ucsd.edu*

Received February 17, 2010; accepted April 6, 2010;
posted April 15, 2010 (Doc. ID 124335); published May 14, 2010

We derive an approach for imaging attenuative sample parameters with a confocal scanning system. The technique employs computational processing to form the estimate in a pixel-by-pixel manner from measurements at the Fourier plane, rather than detecting a focused point at a pinhole. While conventional imaging system analysis and design assumes an independent scatterer at each point in the sample, attenuation must be treated with a tomographic approach. We show that a simple estimator may be derived that requires minimal computation and compare it to the conventional pinhole estimate. The method can potentially be used to image attenuation parameters and occlusion with incoherent detection, as well as refractive index variation with coherent detection, and could potentially allow for video rate imaging due to its computational simplicity. We further consider the application to the problem of an unknown gain or phase value, such as in the measurement of phase with a gradient sensor. And we propose a technique to mitigate the effect by computationally imaging off-focus planes. The principles are demonstrated with numerical simulations in two dimensions.

OCIS codes: 180.6900, 110.1758.

1. INTRODUCTION

We consider a simple confocal system such as in Fig. 1(a), a stage-scanning transmissive mode. This may be described as a slight variation upon Minsky's first embodiment of the confocal microscope [1], changed to explicitly show collimated regions between foci. While modern practical systems usually function in a laser-scanned reflective mode [2], we use the system in Fig. 1 because the key aspects of the method presented in this paper are easiest to explain using the system presented here.

So the transmissive confocal system may be described as focusing light with one objective onto the focal plane, then reimaging that same focus with a second objective onto a pinhole. The research presented in this paper, therefore, may be broadly described as an approach to exploit additional collection of light beyond the pinhole. However, rather than collecting the entire image plane in Fig. 1, we prefer to collect the signal in the Fourier plane as shown in Fig. 1(b). Then we wish to form a computational estimate of the "pinhole signal" which is preferable in the case of attenuative samples.

Obviously the function of this type of system is to measure some sample parameter at the focal point, while rejecting effects from points away from the focus. If the sample is treated as a collection of isotropic point scatterers, then the illumination at each point (for a single pinhole measurement) is generally considered as a three-dimensional point-spread function (see, e.g., [2]) due to the illumination objective. Similarly the light collected from each point (again for a single pinhole measurement) is determined by the three-dimensional point-spread function of the measurement objective. So the confocal system produces a measurement whose focal response is essentially "squared" compared to the full-field microscope. The system then is assumed to produce an image whose pixel values relate to the bulk scattering parameter of the sample at each point. This is a useful model for imaging fluorescence of a sample, and that application dominates the use of such microscopes in biomedical imaging.

However, we consider that this model of the sample is incomplete. The sample may absorb light, an effect which is poorly addressed by a technique which rejects scatter. Occlusion, for example, may be considered as an extreme case of absorption. Generally we may describe the effect of absorption with an attenuation coefficient, separate from the scattering coefficient. Also, refractive index variations, both at the sample boundary and within thick samples, may cause varying phase delay in the signal, usually described as "sample-induced" or "specimen-induced" aberrations, and are known to cause significant problems with the image quality [3]. Imaging the refractive index variation as a parameter of interest itself has been the focus of recent research [4–9]. And this too we may address with an attenuation coefficient, in this case an imaginary one. Combined with absorption, the result is a complex attenuation in total. In this paper we will derive an efficient method for imaging this complex attenuation coefficient with a confocal microscope using computational detection, and compare it to the conventional detection approach.

In the next section we will relate the signal at the Fourier plane to the pinhole estimate and to the attenuation coefficient of the sample, thereby showing the assumption made by a conventional confocal system in a measurement of attenuation, for comparison. Then we will directly derive an estimate of the attenuation coefficient at the focus using the Fourier plane signal. Finally we will consider the effect of unknown amplitude and phase on the estimates. This paper provides the first presentation,

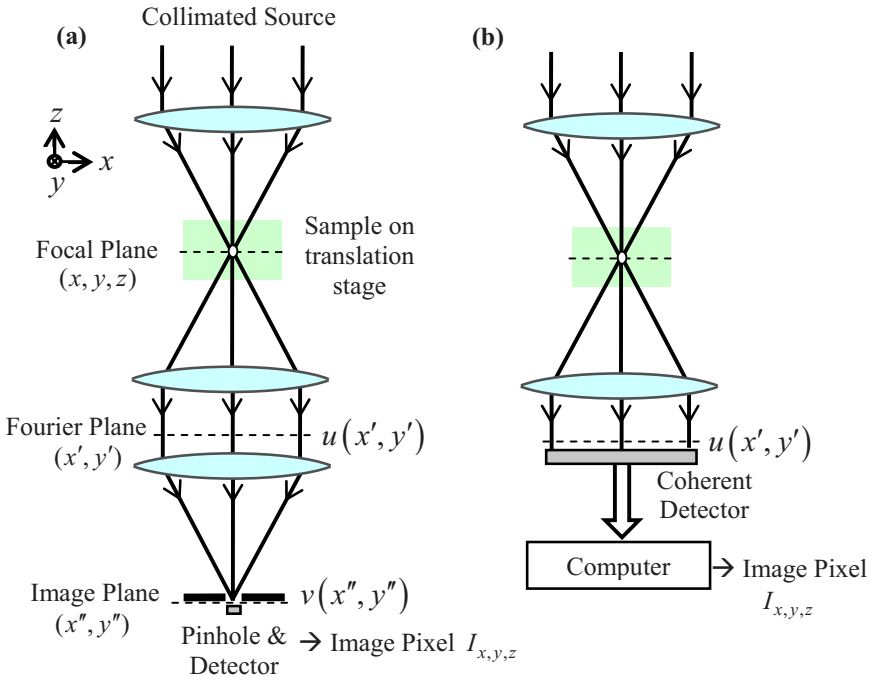

Fig. 1. (Color online) Confocal system. (a) Conventional and (b) computational systems.

to our knowledge, of this simple computation method to estimate the focus in a scanning confocal-based system, as well as the first treatment of an unknown phase or attenuation in the detector in such a system.

2. CONVENTIONAL PINHOLE ESTIMATE

Using the Fraunhofer diffraction theory [10], we can relate the Fourier plane and image plane signals to describe the pinhole estimate. The value detected at the pinhole is the intensity of the image plane signal at $(x'',y'')=(0,0)$. We describe this intensity value as $I(x_0,y_0,z_0)$, where x_0,y_0,z_0 is the location of the translation stage when this intensity is detected at the pinhole. Similarly the complex signals u and v are functions of the focal point location,

$$I(x_0,y_0,z_0)=|v(0,0;x_0,y_0,z_0)|^2 = \left|\int\int_{\text{Aperture}} u(x',y';x_0,y_0,z_0)dx'dy'\right|^2. \tag{1}$$

We consider the interpretation of this value as it relates to bulk properties of the sample. If we assume that by some means we are able to measure the complex signal at the pinhole (such as in [11]), then we have the complex amplitude measurement,

$$A(x_0,y_0,z_0)=\int\int_{\text{Aperture}} u(x',y';x_0,y_0,z_0)dx'dy', \tag{2}$$

where $I(x_0,y_0,z_0)=|A(x_0,y_0,z_0)|^2$. Considering the point-spread function view of imaging, we assume a sample consisting of only a small attenuating region at the focus, which produces an attenuated measurement,

$$A(x_0,y_0,z_0)=e^{-\eta(x_0,y_0,z_0)\Delta x}A_0, \tag{3}$$

using the Beer–Lambert law [12], where A_0 is the amplitude measurement in the absence of the sample attenuation and Δx is the attenuating region thickness (in depth). $\eta(x_0,y_0,z_0)$ is the attenuation coefficient, which may in general be complex. For example the real part is a typical attenuation, and the imaginary part could be the integral along rays of the refractive index variation. This would correspond to using the eikonal approximation for the Helmholtz equation with a varying refractive index and a monochromatic source (see, e.g., [13], Chap. 8).

Solving for η, the sample property of interest, we get

$$\eta(x_0,y_0,z_0)=-\frac{1}{\Delta x}\log A(x_0,y_0,z_0)+\frac{1}{\Delta x}\log A_0 = -\log A(x_0,y_0,z_0), \tag{4}$$

where we have set A_0 and Δx equal to 1 for simplicity. So, by combining Eqs. (2) and (4), we have

$$\eta(x_0,y_0,z_0)=-\log\left\{\int\int_{\text{Aperture}} u(x',y';x_0,y_0,z_0)dx'dy'\right\}. \tag{5}$$

We argue that this is implicitly assumed to be the measurement of attenuation using a conventional confocal system, even when the attenuation is not concentrated at a single point, but present (and perhaps varying) across the entire sample. In such a case a confocal system still provides an image of the attenuation parameter by scanning and sampling this value. But it may not be the best approach for such a sample since attenuation is a multiplicative effect, not linear or shift-invariant.

3. COMPUTATIONAL ESTIMATE

Now we will derive a direct estimator for the attenuation parameter. Figure 2 shows the effect on the Fourier plane signal of attenuation at a given point which is in general away from the focus.

The effect on the Fourier plane signal from a single point attenuation is given by

$$u(x',y';x_0,y_0,z_0) = \begin{cases} A(x_s,y_s,z_s)u_0(x',y'), & \text{if } (x',y') = \dfrac{f}{z_s-z_0}(x_s-x_0,y_s-y_0) \\ u_0(x',y'), & \text{otherwise,} \end{cases} \tag{6}$$

where f is the focal length. By taking the logarithm (we use log to denote the natural logarithm, i.e., base e) we convert this into an additive effect. And for a sample with such points everywhere, described as $a(x,y,z)$, we integrate this over all points on the sample (i.e., let x_s,y_s,z_s range over all x,y,z) to get

$$\log u(x',y';x_0,y_0,z_0) = \int\int\int \delta\left(x' - f\frac{x-x_0}{z-z_0}, y' - f\frac{y-y_0}{z-z_0}\right)\log A(x,y,z)\,dx\,dy\,dz, \tag{7}$$

where δ is the Dirac delta function. We assume that the sample is infinite in size (and simply equal to zero as necessary) so the integrals run over all infinity initially. We have also set u_0, the unattenuated signal, equal to 1 as this term is sample independent and may be measured during system calibration and subtracted out of the measured data. We can simplify this to

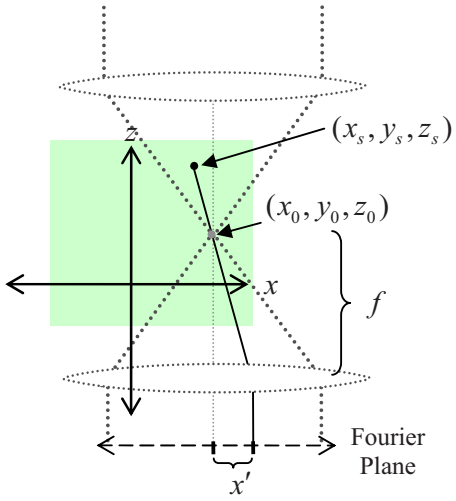

Fig. 2. (Color online) System geometry. The sample is assumed stationary, and the optical system is translated relative to it, as determined by the location of the focus at x_0,y_0,z_0. The optical axis is vertical.

$$\log u(x',y';x_0,y_0,z_0) = \int \log A\left(\frac{x'}{f}(z-z_0) + x_0, \frac{y'}{f}(z-z_0) + y_0, z\right)dz = -\int \eta\left(\frac{x'}{f}(z-z_0) + x_0, \frac{y'}{f}(z-z_0) + y_0, z\right)dz. \tag{8}$$

Equation (8) is an expression for the attenuation at each point in the Fourier plane as a result of the integration of the attenuation along the ray through the sample which intersects that point. One may recognize that such an integral may form the basis for a Radon transform of η, formed by appropriately translating the stage. Hence one approach [to invert Eq. (8) and estimate η] may be to collect the complex Fourier plane signal for a range of points in a scan, and then compute an inverse Radon transform [14] of this data. An approach along these lines was demonstrated in [15].

Our goal here is not to completely invert this expression, but to extract the focal plane $\eta(x,y,z_0)$, a slice of the sample at depth $z=z_0$. We might then collect information at a different depth by physically adjusting the hardware to focus at the new depth. What we gain from this approach is a far simpler computational procedure. We show in Appendix A that by integrating over the aperture for each step in a one-dimensional scan in the x-direction, then high-pass filtering, we are able to retrieve the value of the attenuation coefficient at the focus,

$$\left\{\int\int \log u(x',y';x_0,y_0,z_0)\,dx'\,dy'\right\} * h_x(x_0,y_0) = 2\pi\eta(x_0,y_0,z_0), \tag{9}$$

where "$*$" describes the convolution operation and $h_x(x_0,y_0)$ is the convolution kernel performing a high-pass filtering with respect to the scan direction x.

This result may be computed very efficiently. If we scan the sample along lines in the x-direction, then we must simply filter the pixel values as they are computed. The only additional storage needed beyond the resulting image is for the taps of the filter. Note that we do not store aperture pixels in the filter taps, just the integrated total for each point in the scan.

In Appendix B we derive the result for estimating an off-focus plane (see Fig. 3),

$$\left\{\int \log u\left(x',y';x_0,y_0,\frac{\Delta z}{f}x' - x_0, \frac{\Delta z}{f}y' - y_0\right)dx'\right\} * h_x(x_0,y_0) = 2\pi\eta(x_0,y_0,z_0-\Delta z). \tag{10}$$

This is essentially a filtered backprojection. We must high-pass filter a collection of aperture measurements, then interpolate a ray through that filtered data to the result. Clearly this is a much more computationally intensive operation.

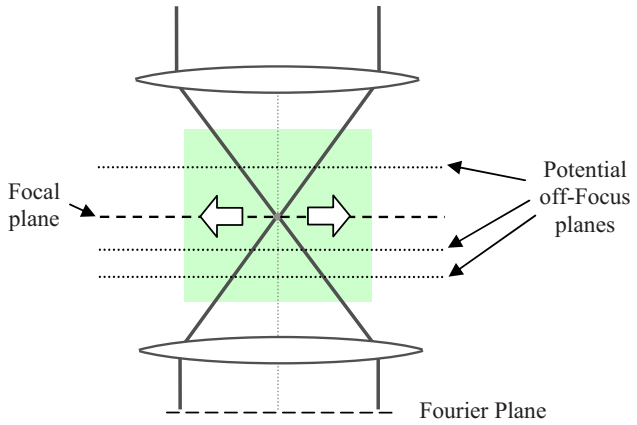

Fig. 3. (Color online) Focal plane and "off-focus" planes. The focal plane is scanned at high rate, but we may choose to instead computationally form an image at a different plane.

Table 1. Comparison of Estimates

Standard pinhole estimate	$\eta(x,y,z)=-\log\{\int u_{x,y,z}\}$
Computational pinhole estimate	$\eta(x,y,z)=-\{\int \log u_{x,y,z}\}*h_x$

We compare the computational estimate of the attenuation coefficient at the focus to the conventional pinhole estimate in Table 1, where the integrals refer to integration over the aperture in both cases. So the pinhole estimate of the pixel is the logarithm of the integrated aperture signal (performed with an objective lens), while the new estimate is the filtered integral of the logarithm of the aperture signal, performed computationally.

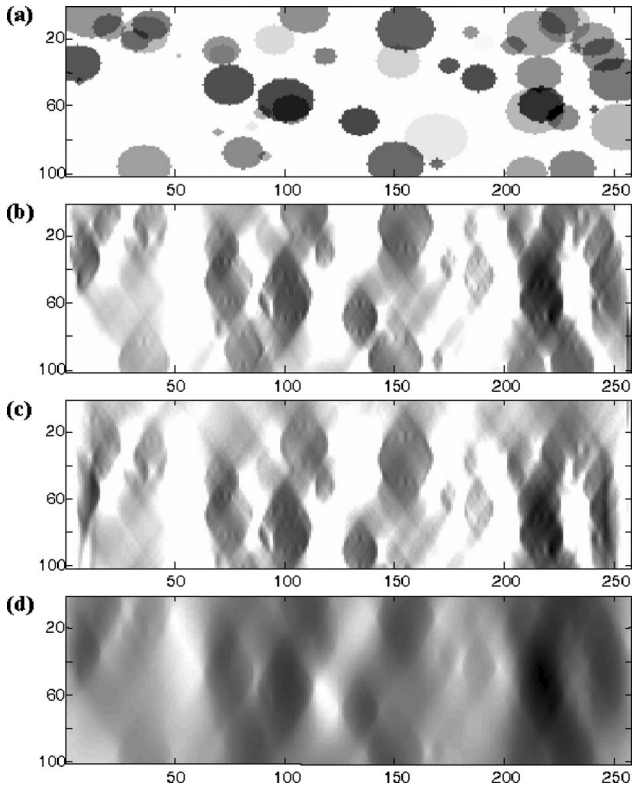

Fig. 4. (a) Synthetic attenuation image, (b) image formed from depth scan of focal plane, (c) image formed from depth scan of off-focus plane, (d) image formed from depth scan of conventional confocal estimate of focal plane.

In Fig. 4 we provide simulation results of the estimates for a two-dimensional situation scanned over depth. Each horizontal line in the images is an estimate of the "plane" corresponding to horizontal lines in the sample; the axial direction is vertical. The estimate was formed for each such line in the simulated sample to demonstrate the depth resolution of the methods. The simulation used a numerical aperture of 0.75.

4. UNKNOWN PHASE OR GAIN

Finally we consider an interesting potential application of off-focus depth sectioning, its ability to filter out an unknown attenuation applied to each aperture measurement. This may result, for example, from the use of a wavefront sensor with a limited or no ability to measure the piston component of the phase. Another example might be a system which uses an adaptive gain control mechanism but does not store the gain values. We will show that while these attenuation terms have the unfortunate result of being indistinguishable from the focal-plane signal, this does allow us to filter them out in principle by sectioning an off-focus plane.

An unknown attenuation effect can be incorporated by applying an amplitude term $a(x_0,y_0)$ to the aperture signal $u(x',y')$. $a(x_0,y_0)$ is constant over the aperture but changes for different focal points x_0,y_0 in the scan,

$$u_a(x',y') = a(x_0,y_0)u(x',y'). \tag{11}$$

Clearly the conventional estimate is completely corrupted by this unknown value since it is just the integral over the aperture. Further we can see that such an error term is indistinguishable from a focal-plane signal with the tomographic estimate. By taking the log,

$$\begin{aligned}\log u_a(x',y') &= \log a(x_0,y_0) + \log u(x',y') \\ &= \log a(x_0,y_0) - \int \eta\left(\frac{x'}{f}(z-z_0)\right. \\ &\quad \left. + x_0, \frac{y'}{f}(z-z_0) + y_0, z\right) dz. \end{aligned} \tag{12}$$

Then as we estimate the depth section at the focus by integrating over the aperture and high-pass filtering, we get

$$\begin{aligned}&\left\{\int\int \log u_a(x',y';x_0,y_0,z_0)dx'dy'\right\} * h_x(x_0,y_0) \\ &= \left\{\int\int \log a(x_0,y_0,z_0)dx'dy'\right\} * h_x(x_0,y_0) \\ &\quad + \left\{\int\int \log u(x',y';x_0,y_0,z_0)dx'dy'\right\} * h_x(x_0,y_0) \\ &= N^2 \log a(x_0,y_0,z_0) * h_x(x_0,y_0) + 2\pi\eta(x_0,y_0,z_0), \end{aligned} \tag{13}$$

where N^2 is the area of the aperture. So a high-pass filtered version of the unknown attenuation term is added directly to the focal result.

Now for the off-focus depth section,

$$\frac{1}{(2\pi)^2}\int\int\int \frac{k_x}{f} e^{-j(\Delta z/f)(x'k_x+y'k_y)} \times\{\log u_a(x',y')\}e^{j(k_x x_0+k_y y_0)}dx'dk_x dk_y = \text{error term} + 2\pi\eta(x_0,y_0,z_0-\Delta z), \quad (14)$$

$$\text{error term} = \frac{1}{(2\pi)^2}\int\int\int \frac{k_x}{f} e^{-j(\Delta z/f)(x'k_x+y'k_y)} \times\left\{\int\int \log a(x_0,y_0)e^{-j(k_x x_0+k_y y_0)}dx_0dy_0\right\} \times e^{j(k_x x_0+k_y y_0)}dx'dk_x dk_y$$

$$= \frac{1}{(2\pi)^2}\int\int \frac{k_x}{f} e^{-j(\Delta z/f)y'k_y}\left\{\int e^{-j(\Delta z/f)x'k_x}dx'\right\} \times\left\{\int\int \log a(x_0,y_0)e^{-j(k_x x_0+k_y y_0)}dx_0dy_0\right\} \times e^{j(k_x x_0+k_y y_0)}dk_x dk_y. \quad (15)$$

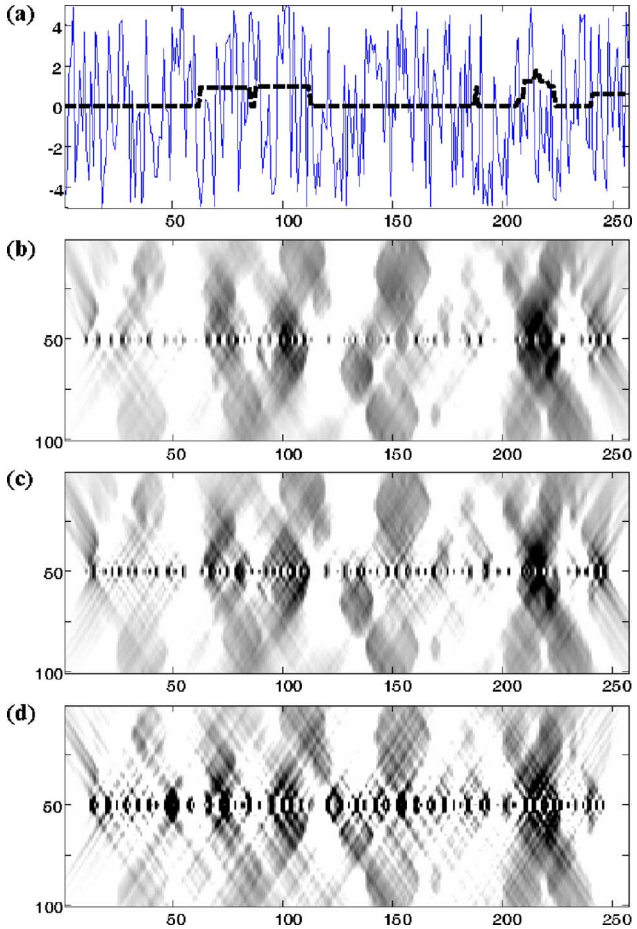

Fig. 5. (Color online) Simulation of application of random attenuation (at given multiples larger than true signal) to each aperture measurement. (a) Example of random attenuation values (solid curve) versus true attenuation (dashed curve) for 5×, (b) image formed for 5×, (c) image formed for 10×, (d) image formed for 25×.

We set $y'=0$ for simplicity (see Appendix B). The error term resulting from the unknown attenuation can be described as the inverse Fourier transform of a product of three terms. We write the result as

$$\text{error term} = h_x(x_0,y_0) * w(x_0,y_0) * \log a(x_0,y_0). \quad (16)$$

This term will be significantly attenuated for off-focus points, approaching zero in the large-aperture limit, because the unknown attenuation is convolved with both a high-pass filter, $h_x(x_0,y_0)$, and a low-pass filter, $w(x_0,y_0)$. The low-pass filter is the Fourier transform of the aperture itself.

In Fig. 5 the results of a simulation (numerical aperture of 0.75) are provided with random attenuation applied to the aperture measurement at different multiples of the maximum attenuation in the image. The image is formed for each multiple by computing the focus and all off-focus planes (with the focus always fixed at the center depth, unlike the previous simulation).

As can be seen from the simulation results, the majority of the degradation due to the random attenuation appears at the central horizontal line, which is the focus. For lines away from the center, the estimate given is the corresponding off-focus estimate and the degradation rapidly decreases.

5. DISCUSSION

This paper considered the issue of depth sectioning of an attenuative sample with a scanning approach inspired by the confocal microscope. We discussed the application of the conventional confocal microscope to this situation then compared it to a computational estimate derived from a tomographic perspective. This result was especially interesting in its computational simplicity. A simulation further demonstrated the potential of the approach compared to the conventional confocal estimate. We further considered an interesting application of using the off-focus estimate which, while more computationally difficult to estimate, is able to filter out unknown gain or phase at the aperture signal. A simulation demonstrating this result was also provided.

In deriving the tomographic approach we assumed that the integrals were over the entire axes, which corresponds to an assumption that the numerical aperture covers the entire 180° range. Of course in practice we have a limited aperture and therefore suffer limited-angle artifacts, just as those which arise in conventional computed tomography systems when limited angles of rotation are used [16]. These effects were evident in the simulations. Also the integration limits determine the range of spatial frequencies collected and hence the resolution. See [17] for more discussion of this relationship in a tomographic system.

Further, we note that the assumption of straight rays is an approximation in the case of the index variation. We consider that beyond the initial sample-air or sample-oil interface (which may be treated deterministically as the interface may be assumed to be known), the index variations with biological samples tend to be relatively small

for most structures. There is generally very little reflection from structure boundaries; hence staining is typically needed.

We believe that the computational estimate of the focal plane may allow for video rate depth sectioning due to its simplicity. Certainly the logarithm, integral, and filtering may be performed extremely quickly. The estimation of the complex attenuation requires more careful consideration and effort, perhaps involving phase unwrapping. Finally, while the derivation used stage-scanning, which is difficult to perform at high rates with biological samples, the adaptation to laser-scanning is straightforward. For example, in a laser-scanning system where the beam is translated electromechanically without rotation or shearing, the relative motion is identical.

APPENDIX A: FOCAL POINT

First we review the different coordinate variables involved in Table 2. We start from the logarithmic-aperture signal,

$$\log u(x',y';x_0,y_0,z_0) = -\int \eta\left(\frac{x'}{f}(z-z_0)+x_0,\frac{y'}{f}(z-z_0)+y_0,z\right)dz, \tag{A1}$$

and we use the following form of the projection-slice theorem:

$$\int\int\int \eta(x-az,y-bz,z)e^{-j(k_x x+k_y y)}dxdydz = \tilde{\eta}(k_x,k_y,ak_x+bk_y), \tag{A2}$$

where $\tilde{\eta}(k_x,k_y,k_z)$ is the three-dimensional Fourier transform of $\eta(x,y,z)$. This gives the "slice" in the frequency domain that one would interpolate the Fourier-transformed projection into, with a direct Fourier method.

First we take the two-dimensional Fourier transform of Eq. (A1) with respect to the focal point locations, x_0 and y_0, i.e., $\int\int(\,)e^{-j(k_x x_0+k_y y_0)}dx_0dy_0$. This can be viewed as analogous to taking the Fourier transform of a projection in a direct Fourier method for computed tomography. This yields

$$\int\int \log u(x',y';x_0,y_0,z_0)e^{-j(k_x x_0+k_y y_0)}dx_0dy_0 = \tilde{\eta}\left(k_x,k_y,-\frac{x'}{f}k_x-\frac{y'}{f}k_y\right)e^{-j(z_0/f)(x'k_x+y'k_y)}. \tag{A3}$$

The trailing exponential term on the right-hand side (RHS) results from the shifting property of the Fourier transform.

Table 2. Coordinates Used

x,y,z	The spatial coordinates within which the sample $\eta(x,y,z)$ resides.
x_0,y_0,z_0	The spatial coordinates of the system focus, which vary within x,y,z via scanning.
x',y'	Coordinates of the samples at the Fourier plane, i.e., at the entrance aperture of the microscope objective. Relate as $(x,y,z)=(x_0+x',y_0+y',z_0+f)$.

Now our goal is to extract a single plane of η; hence we will not need to perform the interpolation and inverse Fourier transform in the k_z spatial frequency. We only need to perform a single integral in that axis. This may be achieved a number of ways with Eq. (A3), corresponding to different data collection and image formation techniques.

We multiply Eq. (A3) by $k_x f^{-1}$ and integrate over x'. For the RHS this gives

$$\int \frac{k_x}{f}\{\mathrm{RHS}\}dx' = \int \frac{k_x}{f}\tilde{\eta}\left(k_x,k_y,-\frac{x'}{f}k_x-\frac{y'}{f}k_y\right)e^{-j(z_0/f)(x'k_x+y'k_y)}dx' = -\int \tilde{\eta}(k_x,k_y,\varsigma_x)e^{jz_0\varsigma_x}d\varsigma_x, \tag{A4}$$

where we have made the following change of variables:

$$\varsigma_x = -\frac{x'}{f}k_x-\frac{y'}{f}k_y, \qquad d\varsigma_x = -\frac{k_x}{f}dx'. \tag{A5}$$

Performing the inverse Fourier transform of Eq. (A4) with respect to k_x and k_y, we may extract the value of the attenuation at focus. First for the RHS,

$$\frac{1}{(2\pi)^2}\int\int\int \frac{k_x}{f}\{\mathrm{RHS}\}e^{j(k_x x_0+k_y y_0)}dx'dk_xdk_y = \frac{1}{(2\pi)^2}\int\int\int \tilde{\eta}(k_x,k_y,\varsigma_x)e^{jz_0\varsigma_x}d\varsigma_x e^{j(k_x x_0+k_y y_0)}dk_xdk_y = 2\pi\eta(x_0,y_0,z_0). \tag{A6}$$

Applying the same operations to the left-hand side (LHS) gives

$$\frac{1}{(2\pi)^2}\int\int\int \frac{k_x}{f}\{\mathrm{LHS}\}e^{j(k_x x_0+k_y y_0)}dx'dk_xdk_y = \frac{1}{(2\pi)^2}\int\int\int \frac{k_x}{f}\left\{\int\int \log u(x',y';x_0,y_0,z_0) \times e^{-j(k_x x_0+k_y y_0)}dx_0dy_0\right\}e^{j(k_x x_0+k_y y_0)}dx'dk_xdk_y = \left\{\int \log u(x',y';x_0,y_0,z_0)dx'\right\} * h_x(x_0,y_0), \tag{A7}$$

where we have written the LHS as a convolution with the filter

$$h_x(x_0,y_0) \leftrightarrow H_x(k_x,k_y) = \frac{k_x}{f}. \tag{A8}$$

And so the combined result is

$$\left\{ \int \log u(x',y';x_0,y_0,z_0)dx' \right\} * h_x(x_0,y_0) = 2\pi\eta(x_0,y_0,z_0). \tag{A9}$$

This result is independent of y'. In other words, within an aperture of pixels enumerated by x' and y' we have integrated over x' and have computed a value which we expect to be constant over y'. Therefore we may integrate this dimension as well (to average out noise, for example) yielding an estimate based simply on the sum over the entire aperture,

$$\left\{ \int\int \log u(x',y';x_0,y_0,z_0)dx'dy' \right\} * h_x(x_0,y_0) = 2\pi\eta(x_0,y_0,z_0). \tag{A10}$$

APPENDIX B: OFF-FOCUS POINTS

Returning to Eq. (A3), which we reproduce here,

$$\int\int \log u(x',y';x_0,y_0,z_0)e^{-j(k_x x_0+k_y y_0)}dx_0dy_0 = \tilde{\eta}\left(k_x,k_y,-\frac{x'}{f}k_x-\frac{y'}{f}k_y\right)e^{-j(z_0/f)(x'k_x+y'k_y)}, \tag{B1}$$

we may perform an estimate of points off focus by applying the linear phase $\exp\{-j\Delta z f^{-1}(x'k_x+y'k_y)\}$ (chosen to achieve translation Δz in the z-direction) to both sides prior to the integration over x' and the inverse Fourier transforms. Repeating the steps from Appendix A, but with the shifted coordinate $(z_0-\Delta z)$,

$$\begin{aligned}
&\frac{1}{(2\pi)^2}\int\int\int \frac{k_x}{f}e^{-j(\Delta z/f)(x'k_x+y'k_y)}\{\mathrm{RHS}\}e^{j(k_x x_0+k_y y_0)}dx'dk_xdk_y \\
&= \frac{1}{(2\pi)^2}\int\int\int \frac{k_x}{f}e^{-j(\Delta z/f)(x'k_x+y'k_y)}\left\{\tilde{\eta}\left(k_x,k_y,-\frac{x'}{f}k_x-\frac{y'}{f}k_y\right)e^{-j(z_0/f)(x'k_x+y'k_y)}\right\}e^{j(k_x x_0+k_y y_0)}dx'dk_xdk_y \\
&= \frac{1}{(2\pi)^2}\int\int\int \frac{k_x}{f}\left\{\tilde{\eta}\left(k_x,k_y,-\frac{x'}{f}k_x-\frac{y'}{f}k_y\right)e^{-j[(z_0+\Delta z)/f](x'k_x+y'k_y)}\right\}e^{j(k_x x_0+k_y y_0)}dx'dk_xdk_y \\
&= \frac{1}{(2\pi)^2}\int\int\int \tilde{\eta}(k_x,k_y,\varsigma_x)e^{j(z_0+\Delta z)\varsigma_x}d\varsigma_x e^{j(k_x x_0+k_y y_0)}dk_xdk_y \\
&= 2\pi\eta(x_0,y_0,z_0+\Delta z).
\end{aligned} \tag{B2}$$

Applying the same operations to the LHS of Eq. (A3),

$$\begin{aligned}
&\frac{1}{(2\pi)^2}\int\int\int \frac{k_x}{f}e^{-j(\Delta z/f)(x'k_x+y'k_y)}\{\mathrm{LHS}\}e^{j(k_x x_0+k_y y_0)}dx'dk_xdk_y \\
&= \frac{1}{(2\pi)^2}\int\left\{\int\int \frac{k_x}{f}\exp\left[-j\left(\frac{\Delta z}{f}x'-x_0\right)k_x - j\left(\frac{\Delta z}{f}y'-y_0\right)k_y\right]\{\mathrm{LHS}\}dk_xdk_y\right\}dx'.
\end{aligned} \tag{B3}$$

We have a similar result as derived for the focal plane [see Eq. (A7)], but now with shifted coordinates. So the net result is

$$\left\{\int \log u\left(x',y';\frac{\Delta z}{f}x'-x_0,\frac{\Delta z}{f}y'-y_0,z_0\right)dx'\right\} * h_x(x_0,y_0) = 2\pi\eta(x_0,y_0,z_0-\Delta z). \tag{B4}$$

So we must interpolate, then integrate and high-pass filter. This demonstrates the value gained from sectioning at the focus since collecting an off-focus section requires significantly more storage.

The value of y' (corresponding to pixels in the aperture off-center in the direction perpendicular to the direction of scanning) causes the location of the final measured result to be off-center as well. Assuming that we will collect these values subsequently anyway, such as with a raster scan, we can simply choose $y'=0$ and ignore this issue. In practice we may want to use them to perform averaging between different measurements of the same points taken from different times in the raster scan. In other words, for the focal-plane case different values of y' in the same aperture give redundant measurements of the same measurement point (i.e., the focus), while for the off-focus case the redundancy is between different apertures.

ACKNOWLEDGMENTS

We gratefully acknowledge support from the National Science Foundation (NSF) and the Defense Advanced Research Projects Agency (DARPA).

REFERENCES

1. M. Minsky, "Microscopy apparatus," U.S. patent 3,013,467, 19 December 1961).
2. J.-A. Conchello and J. W. Lichtman, "Optical sectioning microscopy," Nat. Methods **2**, 920–931 (2005).
3. M. J. Booth, M. A. A. Neil, R. Juškaitis, and T. Wilson, "Adaptive aberration correction in a confocal microscope," Proc. Natl. Acad. Sci. U.S.A. **99**, 5788–5792 (2002).
4. A. M. Zysk, J. J. Reynolds, D. L. Marks, P. S. Carney, and S. A. Boppart, "Projected index computed tomography," Opt. Lett. **28**, 701–703 (2003).
5. O. Renaud, J. Viña, Y. Yu, C. Machu, A. Trouvé, H. Van der Voort, B. Chalmond, and S. L. Shorte, "High-resolution 3-D imaging of living cells in suspension using confocal axial tomography," Biotechnol. J. **3**, 53–62 (2008).
6. J. Sharpe, U. Ahlgren, P. Perry, B. Hill, A. Ross, J. Hecksher-Sorensen, R. Baldock, and D. Davidson, "Optical projection tomography as a tool for 3D microscopy and gene expression studies," Science **296**, 541–545 (2002).
7. S. Kikuchi, K. Sonobe, and N. Ohyama, "Three-dimensional microscopic computed tomography based on generalized Radon transform for optical imaging systems," Opt. Commun. **123**, 725–733 (1996).

8. G. N. Vishnyakov, G. G. Levin, and V. L. Minaev, "Tomographic interference microscopy of living cells," Microscopy and Analysis **18**, 19–21 (2004).
9. N. Lue, W. Choi, G. Popescu, K. Badizadegan, R. R. Dasari, and M. S. Feld, "Synthetic aperture tomographic phase microscopy for 3D imaging of live cells in translational motion," Opt. Express **16**, 16240–16246 (2008).
10. J. Goodman, *Introduction to Fourier Optics*, 3rd ed. (Roberts & Company, 2005).
11. T. Wilson, "Coherent methods in confocal microscopy," IEEE Eng. Med. Biol. Mag. **15**, 84–91 (1996).
12. W. F. Cheong, S. A. Prahl, and A. J. Welch, "A review of the optical properties of biological tissues," IEEE J. Quantum Electron. **26**, 2166–2185 (1990).
13. O. K. Ersoy, *Diffraction, Fourier Optics, and Imaging* (Wiley, 2007).
14. S. R. Deans, *The Radon Transform and Some of its Applications* (Wiley, 1983).
15. K. J. Dillon and Y. Fainman, "Computational confocal scanning tomography," in *Computational Optical Sensing and Imaging*, OSA Technical Digest (CD) (Optical Society of America, 2009), paper JTuC7.
16. M. E. Davison, "The ill-conditioned nature of the limited angle tomography problem," SIAM J. Appl. Math. **43**, 428–448 (1983).
17. K. J. Dillon and Y. Fainman, "Computational confocal tomography for simultaneous reconstruction of object, occlusions, and aberrations," Appl. Opt. **49**, 2529–2538 (2010).